The Astrophysical Journal, 594:279–293, 2003 September 1

A QUANTITATIVE COMPARISON OF THE SMALL MAGELLANIC CLOUD, LARGE MAGELLANIC CLOUD, AND MILKY WAY ULTRAVIOLET TO NEAR-INFRARED EXTINCTION CURVES[1]

Karl D. Gordon,[2] Geoffrey C. Clayton,[3] K. A. Misselt,[2] Arlo U. Landolt,[3] and Michael J. Wolff[4]

Received 2002 July 19; accepted 2003 May 7

ABSTRACT

We present an exhaustive quantitative comparison of all the known extinction curves in the Small and Large Magellanic Clouds (SMC and LMC) with our understanding of the general behavior of Milky Way extinction curves. The R_V-dependent CCM relationship of Cardelli, Clayton, and Mathis and the sample of extinction curves used to derive this relationship are used to describe the general behavior of Milky Way extinction curves. The ultraviolet portion of the SMC and LMC extinction curves are derived from archival *IUE* data, except for one new SMC extinction curve, which was measured using *Hubble Space Telescope* Space Telescope Imaging Spectrograph observations. The optical extinction curves are derived from new (for the SMC) and literature *UBVRI* photometry (for the LMC). The near-infrared extinction curves are calculated mainly from 2MASS photometry supplemented with DENIS and new *JHK* photometry. For each extinction curve, we give $R_V = A(V)/E(B-V)$ and N(H I) values that probe the same dust column as the extinction curve. We compare the properties of the SMC and LMC extinction curves with the CCM relationship three different ways: each curve by itself, the behavior of extinction at different wavelengths with R_V, and the behavior of the extinction curve Fitzpatrick and Massa fit parameters with R_V. As has been found previously, we find that a small number of LMC extinction curves are consistent with the CCM relationship, but the majority of the LMC and all the SMC curves do not follow the CCM relationship. For the first time, we find that the CCM relationship seems to form a bound on the properties of all the LMC and SMC extinction curves. This result strengthens the picture dust extinction curves exhibit of a continuum of properties between those found in the Milky Way and the SMC bar. Tentative evidence based on the behavior of the extinction curves with dust-to-gas ratio suggests that the continuum of dust extinction curves is possibly caused by the environmental stresses of nearby star formation activity.

Subject headings: dust, extinction — galaxies: ISM — Magellanic Clouds — ultraviolet: ISM

1. INTRODUCTION

One of the main tools used in the study of dust grain properties is extinction curves, particularly ultraviolet (UV) extinction curves. In the UV dust extinction is strongest and shows the large variations from region to region in the Milky Way (Witt, Bohlin, & Stecher 1984; Aiello et al. 1988; Fitzpatrick & Massa 1990; Clayton, Gordon, & Wolff 2000), Large Magellanic Cloud (LMC; Clayton & Martin 1985; Fitzpatrick 1986; Misselt, Clayton, & Gordon 1999), and Small Magellanic Cloud (SMC; Lequeux et al. 1982; Prèvot et al. 1984; Gordon & Clayton 1998).

The work of Cardelli, Clayton, & Mathis (1989) found that most of the variation in Milky Way extinction curves could be described by an empirical relationship based on the single parameter $R_V = A_V/E(B-V)$. This was a major step forward in our understanding of dust properties and was possible only because of the existence in the literature of near-infrared photometry for a subset of stars in the Fitzpatrick & Massa (1990) sample. This allowed Cardelli et al. (1989) to determine R_V values and transform the Fitzpatrick & Massa (1990) extinction curves to an absolute scale [i.e., normalized to A_V instead of $E(B-V)$]. These A_V-normalized curves had variations that were correlated with R_V, allowing Cardelli et al. (1989) to empirically derive the R_V-dependent CCM relationship. Since the R_V value is a rough measure of average dust grain size, this gave a physical basis for the variations in extinction curves. It is worth noting that significant small deviations from the CCM relationship are seen for individual sight lines (Mathis & Cardelli 1992).

The one caveat on the result of Cardelli et al. (1989) is that the strength of UV dust extinction limits the measurement of UV dust extinction curves to low- to moderate-reddening sight lines. This results in a significant bias in measured UV extinction curves in the Milky Way to regions surrounding the Sun. In the one of the largest detailed studies of UV dust extinction curves in the Milky Way to date, Fitzpatrick & Massa (1990) presented curves for 78 sight lines, and the average distance probed was 1.3 kpc. The CCM relationship was derived from a subset of the Fitzpatrick & Massa (1990) sample and, as such, this relationship might be valid only for dust in our region of the Milky Way. Clayton et al. (2000) tested the validity of the CCM relationship for a larger region of the Milky Way by measuring UV extinction curves along very low-density sight lines. The 26 extinction curves in their sample had an average distance of 5.2 kpc. They found that 19 of the 26 extinction curves in their sample were qualitatively consistent with the CCM relationship. The shapes of the remaining seven curves were not

[1] Partially based on observations made with the NASA/ESA Hubble Space Telescope, obtained at the Space Telescope Science Institute, which is operated by the Association of Universities for Research in Astronomy, Inc., under NASA contract NAS 5-26555. These observations are associated with proposal 8198.

[2] Steward Observatory, University of Arizona, Tucson, 933 North Cherry Avenue, AZ 85721; kgordon@as.arizona.edu, kmisselt@as.arizona.edu.

[3] Department of Physics and Astronomy, Louisiana State University, Baton Rouge, LA 70803; gclayton@fenway.phys.lsu.edu, landolt@rouge.phys.lsu.edu.

[4] Space Science Institute, 1540 30th Street, Suite 23, Boulder, CO 80303-1012; wolff@colorado.edu.

described by the CCM relationship and were qualitatively similar to those seen in the part of the Large Magellanic Cloud (Misselt et al. 1999) associated with the LMC2 supershell (near the 30 Dor star formation region). These seven curves were all clustered in the same region in the sky, and this sight line through the galaxy displays evidence for shocked dust (Clayton et al. 2000).

The CCM relationship seems to be a good description of Milky Way extinction curves with a few exceptions. This raises the question: Does the CCM relationship describe the dust outside the Milky Way? In other words, are the extinction curves in other galaxies quantitatively similar to those in the Milky Way? Only in the Magellanic Clouds can this question be answered as these are the only two galaxies with reliably measured UV extinction curves. A full answer to this question requires R_V values for all the Magellanic Cloud extinction curves, and this has been possible only with the recent release of the 2MASS observations of the Magellanic Clouds. This is the motivation for this paper. Even without all the needed R_V measurements, previous work has gone a long way in answering the above question. It was quickly realized with the first few measured extinction curves in the LMC and SMC that the Clouds had curves that were similar to Milky Way curves, as well as curves that were quite different. For example, the sight lines toward the LMC star Sk $-69°108$ (Nandy & Morgan 1978) and the SMC star AzV 456 (Lequeux et al. 1982) display Milky Way–like extinction curves. On the other hand, sight lines near 30 Dor in the LMC (Clayton & Martin 1985; Fitzpatrick 1986) and in the star-forming bar of the SMC (Prèvot et al. 1984) show definitely non–Milky Way–like extinction curves, especially in their 2175 Å bump and far-UV rise strengths.

To move from a qualitative to a quantitative comparison of Magellanic Cloud and Milky Way extinction curves, R_V values are needed for each extinction curve. This allows for the normalization of the extinction curves by A_V instead of the usual $E(B-V)$, which the Cardelli et al. (1989) work proved was vitally important in understanding the true differences between extinction curves. While the studies of Gordon & Clayton (1998) and Misselt et al. (1999) concentrated on deriving all the UV extinction curves possible with *International Ultraviolet Explorer* (*IUE*) archival data in the SMC and LMC, respectively, they also presented R_V values for a subset of the SMC and LMC curves. Ideally, the R_V values for each extinction curve should be derived from near-infrared photometry of both the reddened and comparison stars that make up each curve. This ensures that the measured extinction curve and R_V value correspond to the same dust column and both are similarly corrected for foreground Milky Way dust. Because of the paucity of near-infrared photometry for their reddened and (especially) comparison stars, a majority of the R_V values presented in Gordon & Clayton (1998) and Misselt et al. (1999) were based on assumed near-infrared intrinsic colors. In addition, the colors of the reddened stars were not corrected for Milky Way foreground dust. This interjected a significant error in the R_V values. For example, the foreground extinction can be up to 25% of the total extinction for the LMC extinction curves (Misselt et al. 1999). This results in significant differences between R_V values reported in these two studies and previous work (Morgan & Nandy 1982). The release of the 2MASS data for the Magellanic Clouds makes it possible to correctly and accurately compute R_V values for all the known extinction curves in the Magellanic Clouds (Gordon & Clayton 1998; Misselt et al. 1999) by using the 2MASS near-infrared photometry of the reddened and comparison stars.

We combine archival *IUE* ultraviolet spectra, optical photometry, and the 2MASS (Skrutskie et al. 1997) and DENIS (Epchtein et al. 1999; Cioni et al. 2000) near-infrared photometry with new *Hubble Space Telescope* (*HST*) Space Telescope Imaging Spectrograph (STIS) ultraviolet spectroscopy and optical photometry to derive ultraviolet through near-infrared extinction curves for 24 sight lines in the Magellanic Clouds in § 2. In the same section, we also measure the R_V and H I column for all 24 extinction curves. In § 3, we quantitatively compare Milky Way and Magellanic Cloud extinction curves as well as discuss various average Magellanic Cloud extinction curves and the existence or lack thereof of the 2175 Å bump in the SMC bar.

2. DATA

We present data on all the sight lines in the Magellanic Clouds that have UV extinction curves. The sight lines include 23 on the basis of *IUE* data that have been published previously (Gordon & Clayton 1998; Misselt et al. 1999) and one on the basis of STIS data that are published for the first time in this paper. For each sight line, we have gathered UV spectra and optical and near-infrared photometry for both the reddened and comparison stars. From these data, we have constructed UV to near-IR extinction curves by using the standard-pair method and measured R_V and $N(\mathrm{H\ I})$ values for each sight line.

2.1. *Optical and Near-Infrared Photometry*

The optical and near-infrared photometry for the reddened and comparison stars is given in Table 1. *UBVRI* photometric data for all the SMC stars, as well as two of the LMC stars (Sk $-67°36$ and Sk $-68°26$), were obtained on observing runs during 1998 August and September, 1999 January, and 2001 August. The data were acquired at the 1.5 m telescope of the Cerro Tololo Inter-American Observatory (CTIO). A C31034A GaAs photomultiplier, *UBVRI* filter set 3, and the standard photoelectric data acquisition system were used. Extinction and transformation relations, including nonlinear transformation relations, were applied to the instrumental data. The final magnitudes and color indices are on the photometric system defined by Landolt (1992). The *UBV* optical photometry for the remainder of the LMC stars was taken from Misselt et al. (1999).

The *JHK* near-infrared photometry for most of the SMC and LMC stars was taken from the results of the 2MASS project (Skrutskie et al. 1997). The *JHK* photometry for the SMC stars AzV 456 and AzV 462 was taken from Bouchet et al. (1985). For two of the three LMC stars without 2MASS photometry, we used the DENIS (Epchtein et al. 1999; Cioni et al. 2000) *JK* photometry converted to the 2MASS system (Cutri et al. 2000). For the one LMC star without 2MASS or DENIS photometry because of a nearby saturating star, we used *JHK* images of Sk $-68°26$ and its surrounding region that were taken using the Cerro Tololo InfraRed IMager at the CTIO 1.5 m telescope. These images were taken on 1999 December 15 in nonphotometric weather, and each band was observed four times, offsetting between positions for a total exposure time of 4 s. The field

TABLE 1

STELLAR PHOTOMETRY

Star	V	$B-V$	$U-B$	$V-R$	$V-I$	J	H	K_s
				SMC				
AzV 18	12.420 ± 0.044	0.041 ± 0.006	−0.794 ± 0.021	0.069 ± 0.005	0.123 ± 0.008	12.368 ± 0.032	12.336 ± 0.030	12.261 ± 0.033
AzV 23	12.244 ± 0.004	0.084 ± 0.002	−0.672 ± 0.008	0.092 ± 0.003	0.188 ± 0.006	12.011 ± 0.032	11.923 ± 0.025	11.913 ± 0.035
AzV 70	12.413 ± 0.013	−0.154 ± 0.013	−1.003 ± 0.016	−0.046 ± 0.011	−0.124 ± 0.017	12.711 ± 0.032	12.765 ± 0.033	12.832 ± 0.039
AzV 214	13.416 ± 0.013	0.038 ± 0.007	−0.803 ± 0.007	0.065 ± 0.004	0.129 ± 0.007	13.357 ± 0.035	13.374 ± 0.039	13.312 ± 0.048
AzV 289	12.396 ± 0.026	−0.118 ± 0.009	−0.984 ± 0.013	−0.032 ± 0.005	−0.111 ± 0.014	12.657 ± 0.024	12.670 ± 0.038	12.718 ± 0.035
AzV 380	13.534 ± 0.007	−0.109 ± 0.010	−0.918 ± 0.009	−0.013 ± 0.008	−0.037 ± 0.009	13.747 ± 0.031	13.781 ± 0.045	13.841 ± 0.057
AzV 398	13.889 ± 0.026	0.100 ± 0.022	−0.820 ± 0.021	0.107 ± 0.007	0.150 ± 0.032	13.687 ± 0.029	13.590 ± 0.038	13.374 ± 0.042
AzV 404	12.197 ± 0.009	−0.098 ± 0.006	−0.825 ± 0.005	0.000 ± 0.004	−0.017 ± 0.003	12.394 ± 0.033	12.438 ± 0.038	12.409 ± 0.037
AzV 456	12.888 ± 0.019	0.109 ± 0.009	−0.785 ± 0.015	0.085 ± 0.002	0.162 ± 0.006	12.820 ± 0.020	12.800 ± 0.025	12.800 ± 0.019
AzV 462	12.566 ± 0.017	−0.126 ± 0.012	−0.914 ± 0.014	−0.039 ± 0.004	−0.124 ± 0.005	12.890 ± 0.020	12.940 ± 0.025	12.950 ± 0.019
				LMC				
Sk −65°15	12.140 ± 0.020	−0.100 ± 0.020	−0.920 ± 0.040	...	...	12.417 ± 0.025	12.409 ± 0.026	12.423 ± 0.030
Sk −65°63	12.560 ± 0.020	−0.160 ± 0.020	−1.020 ± 0.040	...	...	12.933 ± 0.033	12.941 ± 0.036	13.024 ± 0.045
Sk −66°19	12.790 ± 0.020	0.120 ± 0.020	−0.780 ± 0.040	...	...	12.496 ± 0.031	12.382 ± 0.028	12.359 ± 0.040
Sk −66°35	11.550 ± 0.020	−0.070 ± 0.020	−0.880 ± 0.040	...	...	11.732 ± 0.027	11.725 ± 0.024	11.700 ± 0.034
Sk −66°88	12.700 ± 0.020	0.200 ± 0.020	−0.650 ± 0.040	...	...	12.170 ± 0.027	12.089 ± 0.030	11.945 ± 0.033
Sk −66°106	11.720 ± 0.020	−0.080 ± 0.020	−0.910 ± 0.040	...	...	11.919 ± 0.028	11.931 ± 0.033	11.918 ± 0.031
Sk −66°118	11.810 ± 0.020	−0.050 ± 0.020	−0.860 ± 0.040	...	...	12.072 ± 0.026	11.984 ± 0.035	12.013 ± 0.036
Sk −66°169	11.560 ± 0.020	−0.130 ± 0.020	−1.000 ± 0.040	...	...	11.862 ± 0.033	11.895 ± 0.038	11.882 ± 0.040
Sk −67°2	11.260 ± 0.020	0.080 ± 0.020	−0.690 ± 0.040	...	...	11.054 ± 0.024	11.010 ± 0.034	10.895 ± 0.030
Sk −67°5	11.340 ± 0.020	−0.120 ± 0.020	−0.950 ± 0.040	...	...	11.621 ± 0.028	11.623 ± 0.031	11.636 ± 0.032
Sk −67°36	12.029 ± 0.003	−0.090 ± 0.007	−0.853 ± 0.008	−0.003 ± 0.006	−0.013 ± 0.011	12.095 ± 0.031	12.116 ± 0.026	12.174 ± 0.035
Sk −67°78	11.260 ± 0.020	−0.040 ± 0.020	−0.730 ± 0.040	...	...	11.439 ± 0.058	...	11.258 ± 0.031
Sk −67°100	11.950 ± 0.020	−0.090 ± 0.020	−0.860 ± 0.040	...	...	12.158 ± 0.031	12.235 ± 0.031	12.204 ± 0.038
Sk −67°168	12.080 ± 0.020	−0.170 ± 0.020	−1.000 ± 0.040	...	...	12.491 ± 0.029	12.461 ± 0.033	12.528 ± 0.036
Sk −67°228	11.490 ± 0.020	−0.050 ± 0.020	−0.820 ± 0.040	...	...	11.574 ± 0.033	11.576 ± 0.035	11.529 ± 0.037
Sk −67°256	11.900 ± 0.020	−0.080 ± 0.020	−0.890 ± 0.040	...	...	11.938 ± 0.032	12.047 ± 0.039	11.955 ± 0.031
Sk −68°23	12.810 ± 0.020	0.220 ± 0.020	−0.610 ± 0.040	...	...	12.180 ± 0.027	12.047 ± 0.028	11.958 ± 0.034
Sk −68°26	11.630 ± 0.003	0.116 ± 0.002	−0.776 ± 0.001	0.115 ± 0.003	0.238 ± 0.007	11.410 ± 0.060	11.280 ± 0.040	11.150 ± 0.050
Sk −68°40	11.710 ± 0.020	−0.070 ± 0.020	−0.790 ± 0.040	...	...	11.706 ± 0.027	11.716 ± 0.037	11.760 ± 0.030
Sk −68°41	12.000 ± 0.020	−0.140 ± 0.020	−0.960 ± 0.040	...	...	12.204 ± 0.027	12.284 ± 0.036	12.242 ± 0.032
Sk −68°129	12.770 ± 0.020	0.030 ± 0.020	−0.840 ± 0.040	...	...	12.566 ± 0.032	12.572 ± 0.034	12.514 ± 0.041
Sk −68°140	12.720 ± 0.020	0.060 ± 0.020	−0.830 ± 0.040	...	...	12.479 ± 0.018	12.432 ± 0.018	12.380 ± 0.020
Sk −68°155	12.720 ± 0.020	0.030 ± 0.020	−0.820 ± 0.040	...	...	12.723 ± 0.033	12.630 ± 0.039	12.669 ± 0.035
Sk −69°108	12.100 ± 0.020	0.270 ± 0.020	−0.490 ± 0.040	...	...	11.530 ± 0.029	...	11.263 ± 0.015
Sk −69°206	12.840 ± 0.020	0.140 ± 0.020	−0.760 ± 0.040	...	...	12.408 ± 0.033	12.382 ± 0.037	12.257 ± 0.043
Sk −69°210	12.590 ± 0.020	0.360 ± 0.020	−0.590 ± 0.040	...	...	11.796 ± 0.036	11.711 ± 0.033	11.587 ± 0.038
Sk −69°213	11.970 ± 0.020	0.100 ± 0.020	−0.750 ± 0.040	...	...	11.698 ± 0.033	11.713 ± 0.035	11.642 ± 0.037
Sk −69°228	12.120 ± 0.020	0.050 ± 0.020	−0.760 ± 0.040	...	...	12.029 ± 0.034	11.998 ± 0.034	11.937 ± 0.037
Sk −69°256	12.610 ± 0.020	0.030 ± 0.020	−0.830 ± 0.040	...	...	12.799 ± 0.032	12.728 ± 0.047	12.732 ± 0.044
Sk −69°265	11.880 ± 0.020	0.120 ± 0.020	−0.630 ± 0.040	...	...	11.680 ± 0.029	11.628 ± 0.045	11.598 ± 0.037
Sk −69°270	11.270 ± 0.020	0.140 ± 0.020	−0.520 ± 0.040	...	...	11.009 ± 0.036	10.989 ± 0.037	10.936 ± 0.036
Sk −69°279	12.790 ± 0.020	0.050 ± 0.020	−0.840 ± 0.040	...	...	12.701 ± 0.036	12.613 ± 0.051	12.550 ± 0.043
Sk −69°280	12.660 ± 0.020	0.090 ± 0.020	−0.740 ± 0.040	...	...	12.492 ± 0.031	12.451 ± 0.037	12.410 ± 0.037
Sk −70°116	12.050 ± 0.020	0.110 ± 0.020	−0.720 ± 0.040	...	...	11.679 ± 0.034	11.585 ± 0.035	11.520 ± 0.031
Sk −70°120	11.590 ± 0.020	−0.060 ± 0.020	−0.880 ± 0.040	...	...	11.831 ± 0.033	11.803 ± 0.028	11.835 ± 0.036

of view of the co-added images was approximately $200'' \times 200''$. In this region, five of the bright stars have 2MASS observations, and we used these stars to calibrate the *JHK* fluxes for Sk $-68^\circ 26$ by using differential photometry. The uncertainty in these measurements was calculated as the standard deviation of the mean of the five measurements of the *JHK* magnitudes of Sk $-68^\circ 26$, one measurement per 2MASS star.

2.2. *Ultraviolet Spectra*

The UV spectra for all but two of the stars in this paper were taken from archival *IUE* observations. The specific *IUE* observations we used are given by Gordon & Clayton (1998) for the SMC stars and Misselt et al. (1999) for the LMC stars. The individual *IUE* observations were downloaded from the MAST archive at Space Telescope Science Institute (STScI) and were co-added to produce a single spectrum from 1150 to 3225 Å with a resolution of approximately 400. The calibration of these spectra was improved using the results of Massa & Fitzpatrick (2000), who found that the signal-to-noise ratio of *IUE* low-dispersion data could be significantly improved over that provided in the *IUE* archive.

The UV spectra for the final two stars (AzV 23 and AzV 404) were taken with the STIS instrument on *HST* as part of our GO program 8198. The spectra were taken using the $52' \times 0''.5$ slit with the G140L and G230L gratings. The individual observations were co-added to produce spectra extending from 1140 to 3140 Å with a resolution of approximately 1000. These two spectra are presented in Figure 1. The excellent match between the reddened and comparison spectral types can be easily seen in this figure. In addition, the superior nature of STIS ultraviolet spectra compared with *IUE* spectra can be seen by comparing this figure with Figure 1 of Gordon & Clayton (1998), which displays *IUE* spectra for similar spectral type stars.

2.3. *Extinction Curves*

The extinction curves for sight lines in the Magellanic Clouds were derived using the standard-pair method. The reddened/comparison star pairs used are listed in Table 2. We rederived the 23 extinction curves presented in Gordon & Clayton (1998) and Misselt et al. (1999) to take into account the new calibration of *IUE* low-dispersion data (Massa & Fitzpatrick 2000) and the new optical and near-infrared photometry. The effects of the new calibration of the *IUE* spectra on the UV extinction curves was small, mainly reducing the noise in the curves. The one new extinction curve in the SMC for the AzV 23 sight line is presented in Figure 1 at its full spectral resolution.

We calculated all 24 extinction curves and their associated uncertainties as outlined in Gordon & Clayton (1998). In addition, we removed the effects of the Lyα H I absorption by using our measurements of the H I column (see § 2.6). These extinction curves give the difference in extinction between the two sight lines to the reddened and comparison stars. The Milky Way foreground component is effectively removed as long as the reddening due to this component toward the reddened and comparison star pairs are similar (Misselt et al. 1999). This results in an extinction curve that measures dust only in the Magellanic Clouds. All 24 extinction curves are plotted in Figures 2–4.

2.4. *FM Parameters*

We fit each curve with the FM parameterization of the shape of the UV extinction curve (Fitzpatrick & Massa 1990). The FM parameterization is

$$E(x-V)/E(B-V) = C_1 + C_2 x + C_3 D(x, \gamma, x_0) + C_4 F(x) , \quad (1)$$

where $x = \lambda^{-1}$,

$$D(x, \gamma, x_0) = \frac{x^2}{(x^2 - x_0^2)^2 + x^2\gamma^2} , \quad (2)$$

$$F(x) = 0.5392(x - 5.9)^2 + 0.05644(x - 5.9)^3 \quad (3)$$

for $x \geq 5.9$ and $F(x) = 0$ for $x < 5.9$. We determined the FM parameters for the extinction curves by numerically minimizing the χ^2 in a manner similar to that used by Fitzpatrick & Massa (1990). First, x_0 and γ were fixed, and the values of C_1, C_2, C_3, and C_4 were determined by minimizing χ^2. Next, C_1, C_2, C_3, C_4, and γ were fixed, and the value of x_0 was determined by minimizing χ^2. Finally, C_1, C_2, C_3, C_4, and x_0 were fixed, and the value of γ was determined by minimizing χ^2. These two steps were repeated

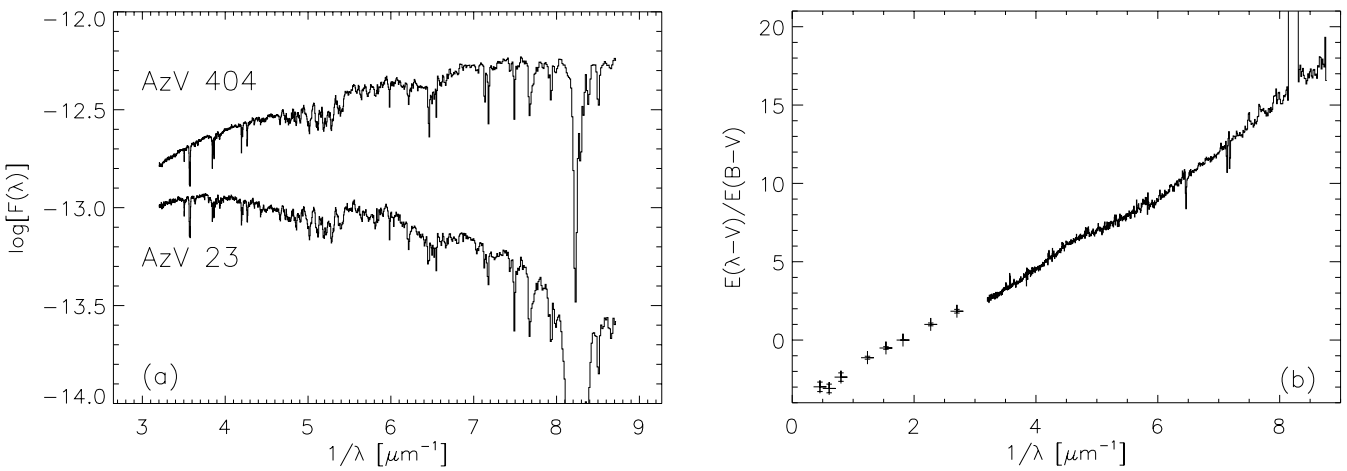

FIG. 1.—(*a*) STIS spectra of AzV 23 and 404; (*b*) resulting extinction curve for AzV 23. The region near Lyα has been corrected for H I absorption.

TABLE 2
EXTINCTION CURVE DATA

Reddened Star	Comparison Star	$E(B-V)$ (mag)	R_V	$N(\mathrm{H\,I})$ (1×10^{21})	$N(\mathrm{H\,I})/A(V)$ (1×10^{21})
		SMC Bar Sample			
AzV 18	AzV 462	0.167 ± 0.013	3.30 ± 0.38	8.50 ± 0.50	15.41 ± 2.33
AzV 23	AzV 404	0.182 ± 0.006	2.65 ± 0.17	8.50 ± 0.50	17.65 ± 1.64
AzV 214	AzV 380	0.147 ± 0.012	2.40 ± 0.30	2.50 ± 0.50	7.08 ± 1.77
AzV 398	AzV 289	0.218 ± 0.024	3.14 ± 0.34	8.00 ± 2.00	11.69 ± 3.43
Average		...	2.74 ± 0.13	...	13.18 ± 1.02
		SMC Wing Sample			
AzV 456	AzV 70	0.263 ± 0.016	2.05 ± 0.17	4.00 ± 0.50	7.40 ± 1.20
		LMC LMC2 Supershell Sample			
Sk $-68^\circ140$	Sk $-68^\circ41$	0.200 ± 0.028	3.27 ± 0.24	4.00 ± 1.00	6.12 ± 1.81
Sk $-68^\circ155$	Sk $-67^\circ168$	0.200 ± 0.028	2.83 ± 0.23	5.00 ± 1.00	8.82 ± 2.28
Sk $-69^\circ228$	Sk $-65^\circ15$	0.150 ± 0.028	3.35 ± 0.33	3.50 ± 0.50	6.97 ± 1.79
Sk $-69^\circ256$	Sk $-68^\circ41$	0.170 ± 0.028	0.64 ± 0.19	2.50 ± 0.50	23.10 ± 9.24
Sk $-69^\circ265$	Sk $-68^\circ40$	0.190 ± 0.028	1.68 ± 0.19	5.00 ± 0.50	15.71 ± 3.35
Sk $-69^\circ270$	Sk $-67^\circ228$	0.190 ± 0.028	2.34 ± 0.22	3.50 ± 1.00	7.86 ± 2.64
Sk $-69^\circ279$	Sk $-65^\circ63$	0.210 ± 0.028	3.33 ± 0.26	4.00 ± 1.00	5.73 ± 1.69
Sk $-69^\circ280$	Sk $-67^\circ100$	0.180 ± 0.028	3.12 ± 0.27	6.00 ± 1.00	10.68 ± 2.62
Sk $-70^\circ116$	Sk $-67^\circ256$	0.190 ± 0.028	3.41 ± 0.27	3.50 ± 0.50	5.39 ± 1.19
Average[a]		...	2.76 ± 0.09	...	6.97 ± 0.67
		LMC Average Sample			
Sk $-66^\circ19$	Sk $-66^\circ169$	0.250 ± 0.028	3.44 ± 0.21	7.00 ± 1.00	8.15 ± 1.57
Sk $-66^\circ88$	Sk $-66^\circ106$	0.280 ± 0.028	3.67 ± 0.19	5.50 ± 0.50	5.35 ± 0.78
Sk $-67^\circ2$	Sk $-66^\circ35$	0.150 ± 0.028	3.62 ± 0.35	1.00 ± 0.50	1.84 ± 1.00
Sk $-68^\circ23$	Sk $-67^\circ36$	0.310 ± 0.021	3.35 ± 0.13	1.50 ± 0.50	1.45 ± 0.50
Sk $-68^\circ26$	Sk $-66^\circ35$	0.186 ± 0.020	3.43 ± 0.24	3.50 ± 0.50	5.48 ± 1.05
Sk $-68^\circ129$	Sk $-68^\circ41$	0.170 ± 0.028	3.36 ± 0.30	4.00 ± 1.00	7.01 ± 2.20
Sk $-69^\circ108$	Sk $-67^\circ78$	0.310 ± 0.028	3.15 ± 0.16	3.00 ± 0.50	3.07 ± 0.61
Sk $-69^\circ206$	Sk -67 5	0.260 ± 0.028	3.68 ± 0.21	8.00 ± 2.00	8.36 ± 2.33
Sk $-69^\circ210$	Sk $-66^\circ118$	0.410 ± 0.028	3.32 ± 0.12	10.00 ± 2.50	7.35 ± 1.93
Sk $-69^\circ213$	Sk $-70^\circ120$	0.160 ± 0.028	3.96 ± 0.36	1.50 ± 0.50	2.37 ± 0.92
Average		...	3.41 ± 0.06	...	3.25 ± 0.28

[a] Excluding Sk $-69^\circ256$.

until χ^2 no longer changed by a significant amount. This three-step method gives a smaller χ^2 than doing a single χ^2 minimization while simultaneously fitting all six parameters. It is worth noting that there are probably only five independent parameters in the FM equation. While all evidence points to C_1 and C_2 being correlated in the Milky Way and the Magellanic Clouds (Fitzpatrick & Massa 1988; Misselt et al. 1999), we have not assumed this correlation.

For the four SMC bar extinction curves, we set $x_0 = 4.6$ and $\gamma = 1.0$ as the weak to nonexistent 2175 Å bumps in these curves preclude fitting all three bump parameters. This allows for a more realistic measurement of the bump strength or an upper limit for these weak-bump sight lines.

The uncertainties in the FM parameters for low $E(B-V)$ sight lines are dominated by the uncertainty in $E(B-V)$ and the random uncertainties of each wavelength point. The uncertainties in the extinction curves were calculated by using equation (2) of Gordon & Clayton (1998). From this equation, it can be seen that an uncertainty in $E(B-V)$ affects the extinction curve in a correlated way. Uncertainties in $E(B-V)$ do not add random noise to each wavelength point, but shift the entire extinction curve up or down. The random uncertainties at each wavelength point contribute a smaller uncertainty, except in the case of x_0 and γ. The contribution of uncertainties in $E(B-V)$ ($\sigma[E(B-V)]$) to the FM parameter uncertainties were calculated by fitting the two additional curves for each measured extinction curve that describe the effects of the $E(B-V)$ uncertainty. These curves are

$$[1+\sigma E(B-V)/E(B-V)]E(x-V)/E(B-V)\ ,$$

$$[1-\sigma E(B-V)/E(B-V)]E(x-V)/E(B-V)\ .$$

The $E(B-V)$ uncertainties in each FM parameter were then $\frac{1}{2}$ the difference between the parameters for these two curves.

The FM parameter uncertainties due to the random uncertainties, σ(random), were calculated using a Monte Carlo approach. Determining the random component of the FM parameter uncertainties is not usually done, but we found that the random component dominates the x_0 and γ uncertainties. This method consisted of generating 100,000 possible FM fits similar to the best FM fit and determining which ones fit equally well within 3 σ by using the F-test where the σ is only that due to random flux uncertainties.

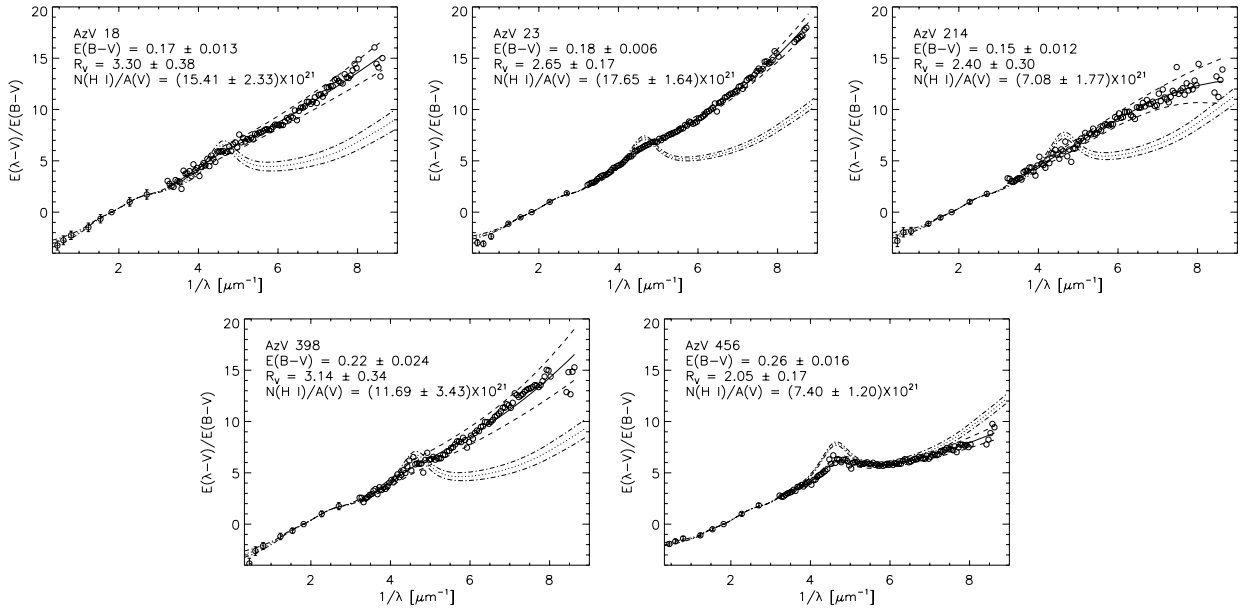

FIG. 2.—SMC extinction curves: best-fit FM90 curve (*solid line*), its uncertainties (*dashed lines*), CCM curve for the measured R_V value (*dotted line*), and its uncertainties (*dot-dashed lines*).

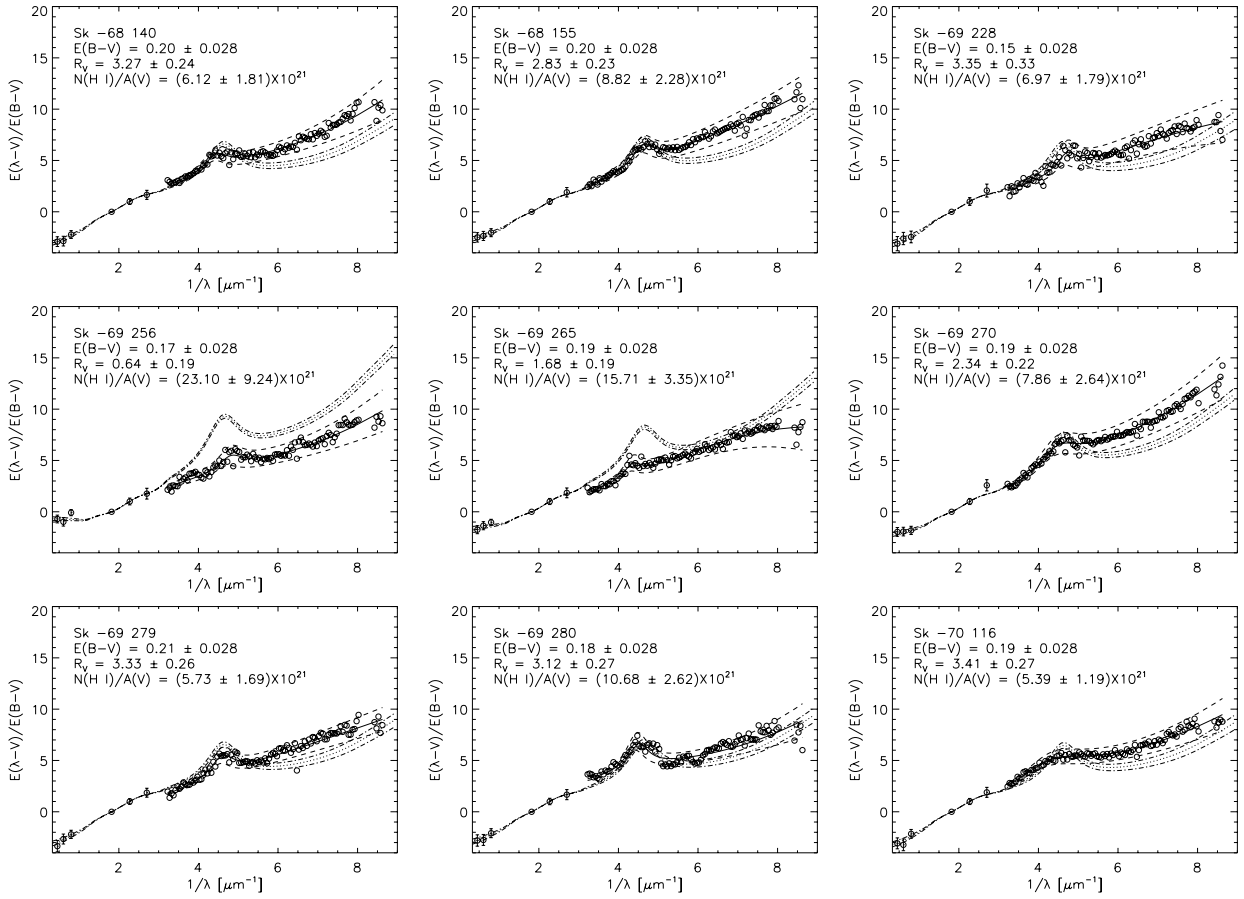

FIG. 3.—LMC extinction curves in the LMC-2 sample: best-fit FM90 curve (*solid line*), its uncertainties, (*dashed lines*), CCM curve for the measured R_V value (*dotted line*), and its uncertainties (*dot-dashed lines*).

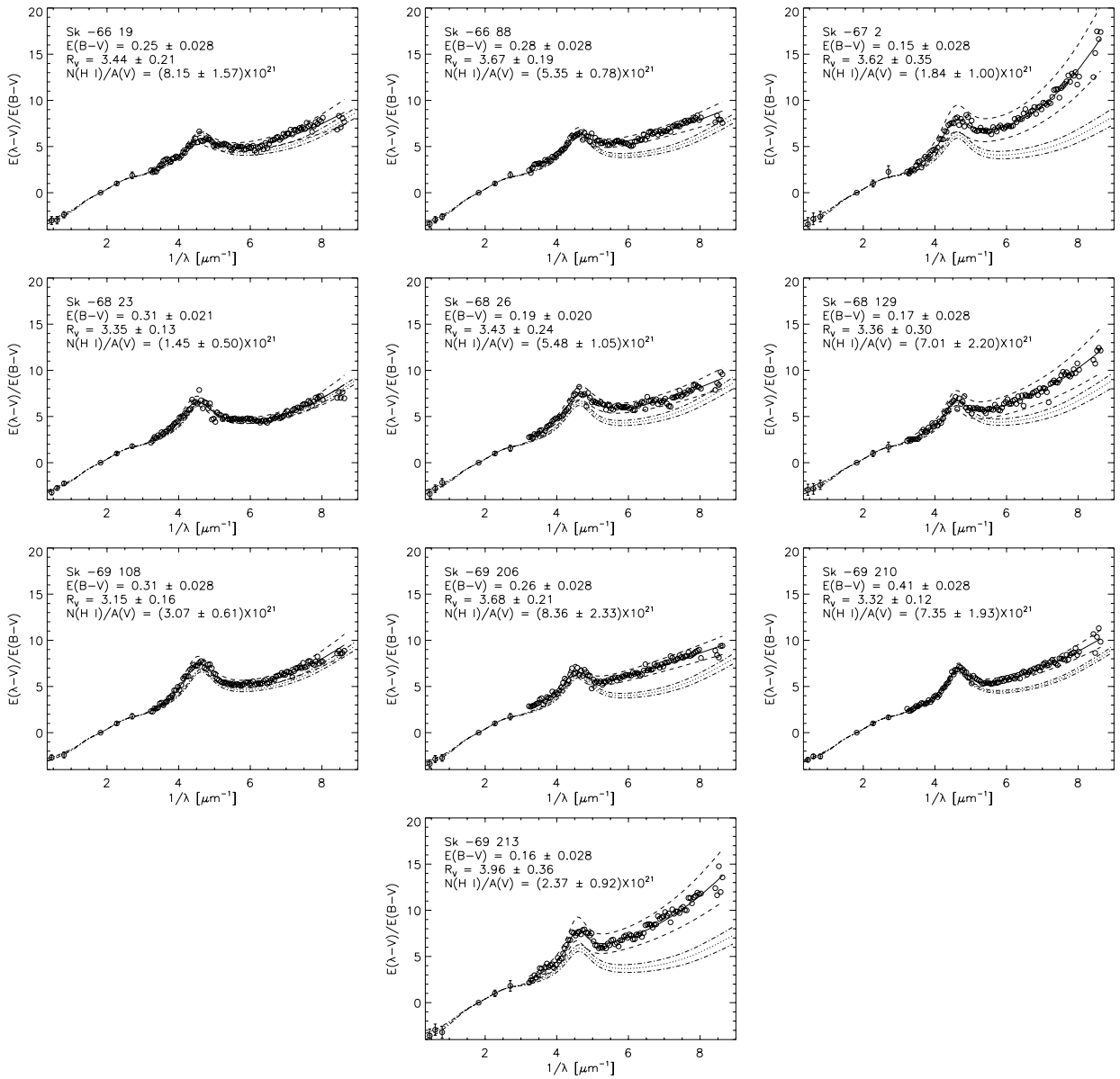

FIG. 4.—LMC extinction curves in the LMC average sample: best-fit FM90 curve (*solid line*), its uncertainties, (*dashed lines*), CCM curve for the measured R_V value (*dotted line*), and its uncertainties (*dot-dashed lines*).

The resulting 1 σ(random) uncertainties were determined by dividing by 3. The reported FM uncertainties (see Table 3) were determined by summing in quadrature the $E(B-V)$-associated ($\sigma[E(B-V)]$) and random [σ (random)] uncertainties. The $E(B-V)$ uncertainties dominate the C_1, C_2, C_3, and C_4 uncertainties, while the random uncertainties dominate the x_0 and γ uncertainties.

2.5. R_V Values

The value of $R_V = A_V/E(B-V)$ for each sight line was determined using a χ^2 minimization method. This method relies on the invariance of the *RIJHK* portion of the extinction curve (Rieke & Lebofsky 1985; Martin & Whittet 1990). The R_V value for each extinction curve is the value that minimizes the χ^2 between the measured *RIJHK* extinction and the Rieke & Lebofsky (1985) curve. The equation giving $\partial\chi^2/\partial R_V = 0$ was solved and the analytic solution for R_V was found. From this equation, the uncertainty for R_V was derived. See the Appendix for details of this derivation. The R_V values and uncertainties are tabulated in Table 2. Our method of using the *RIJHK* extinction curve itself to determine R_V values is different from what is usually done. Usually the observed *VRIJHK* or just *VK* photometry of the reddened star is compared with assumed intrinsic colors (Morgan & Nandy 1982; Cardelli et al. 1989; Gordon & Clayton 1998; Misselt et al. 1999). In the Magellanic Clouds, the reddened stars are usually first corrected for the average Milky Way foreground reddening (Morgan & Nandy 1982). Instead, we have used the measured *VRIJKH* photometry for the matched comparison star and avoided having to assume intrinsic colors of the reddened star. This naturally removes the foreground Milky Way reddening and ensures that the measured R_V value corresponds to the same dust column as the extinction curve. The CCM relationship for these R_V values for each measured extinction

TABLE 3
FM Parameters

Reddened Star	c_1	c_2	c_3	c_4	x_0	γ
SMC Bar Sample						
AzV 18	-4.938 ∓ 0.634	2.267 ± 0.204	0.362 ± 0.190	0.176 ± 0.084	4.600 ± 0.000	1.000 ± 0.000
AzV 23	-5.170 ∓ 0.289	2.382 ± 0.092	0.489 ± 0.125	0.462 ± 0.057	4.600 ± 0.000	1.000 ± 0.000
AzV 214	-4.495 ∓ 0.687	2.264 ± 0.222	-0.123 ± 0.065	-0.435 ± 0.197	4.600 ± 0.000	1.000 ± 0.000
AzV 398	-5.382 ∓ 0.808	2.328 ± 0.276	0.314 ± 0.167	0.263 ± 0.128	4.600 ± 0.000	1.000 ± 0.000
Average	-4.959 ∓ 0.197	2.264 ± 0.040	0.389 ± 0.110	0.461 ± 0.079	4.600 ± 0.000	1.000 ± 0.000
SMC Wing Sample						
AzV 456	-0.856 ∓ 0.246	1.038 ± 0.074	3.215 ± 0.439	0.107 ± 0.038	4.703 ± 0.018	1.212 ± 0.019
LMC LMC2 Supershell Sample						
Sk $-68^\circ 140$	-1.547 ∓ 0.509	1.247 ± 0.197	1.151 ± 0.303	0.357 ± 0.148	4.464 ± 0.039	0.855 ± 0.014
Sk $-68^\circ 155$	-2.689 ∓ 0.487	1.580 ± 0.230	0.923 ± 0.170	0.117 ± 0.049	4.617 ± 0.021	0.693 ± 0.012
Sk $-69^\circ 228$	-2.443 ∓ 0.662	1.373 ± 0.275	0.716 ± 0.234	-0.115 ± 0.065	4.721 ± 0.049	0.643 ± 0.011
Sk $-69^\circ 256$	-1.139 ∓ 0.493	1.101 ± 0.205	0.746 ± 0.271	0.257 ± 0.133	4.817 ± 0.062	0.751 ± 0.013
Sk $-69^\circ 265$	-3.083 ∓ 0.612	1.509 ± 0.237	0.360 ± 0.101	-0.313 ± 0.152	4.363 ± 0.036	0.536 ± 0.009
Sk $-69^\circ 270$	-3.926 ∓ 0.755	1.821 ± 0.281	3.725 ± 0.837	0.208 ± 0.091	4.509 ± 0.034	1.290 ± 0.021
Sk $-69^\circ 279$	-2.669 ∓ 0.551	1.350 ± 0.196	0.978 ± 0.248	0.017 ± 0.009	4.602 ± 0.032	0.708 ± 0.012
Sk $-69^\circ 280$	0.468 ∓ 0.282	0.809 ± 0.142	1.209 ± 0.306	0.232 ± 0.130	4.470 ± 0.032	0.667 ± 0.011
Sk $-70^\circ 116$	-1.707 ∓ 0.567	1.153 ± 0.192	6.557 ± 1.504	0.193 ± 0.080	4.387 ± 0.047	1.878 ± 0.031
Average[a]	-1.475 ∓ 0.152	1.132 ± 0.029	1.463 ± 0.121	0.294 ± 0.057	4.558 ± 0.021	0.945 ± 0.026
LMC Average Sample						
Sk $-66^\circ 19$	-0.724 ∓ 0.282	0.902 ± 0.116	3.036 ± 0.465	0.276 ± 0.118	4.567 ± 0.027	1.132 ± 0.030
Sk $-66^\circ 88$	-0.960 ∓ 0.276	1.051 ± 0.115	2.095 ± 0.310	0.113 ± 0.042	4.580 ± 0.016	0.916 ± 0.015
Sk $-67^\circ 2$	-3.914 ∓ 0.851	1.781 ± 0.347	3.680 ± 0.744	0.884 ± 0.239	4.566 ± 0.014	0.996 ± 0.016
Sk $-68^\circ 23$	-0.152 ∓ 0.070	0.696 ± 0.053	4.647 ± 0.572	0.453 ± 0.108	4.493 ± 0.014	1.135 ± 0.019
Sk $-68^\circ 26$	-1.076 ∓ 0.343	1.082 ± 0.130	4.085 ± 0.621	0.121 ± 0.045	4.622 ± 0.015	1.076 ± 0.018
Sk $-68^\circ 129$	-2.318 ∓ 0.507	1.388 ± 0.243	1.632 ± 0.340	0.468 ± 0.162	4.569 ± 0.019	0.790 ± 0.013
Sk $-69^\circ 108$	-1.262 ∓ 0.327	0.992 ± 0.102	5.046 ± 0.621	0.384 ± 0.101	4.519 ± 0.010	1.079 ± 0.017
Sk $-69^\circ 206$	-1.243 ∓ 0.342	1.217 ± 0.144	1.169 ± 0.204	0.016 ± 0.007	4.500 ± 0.020	0.689 ± 0.011
Sk $-69^\circ 210$	-1.559 ∓ 0.187	1.182 ± 0.087	1.583 ± 0.166	0.307 ± 0.074	4.641 ± 0.007	0.720 ± 0.011
Sk $-69^\circ 213$	-2.791 ∓ 0.703	1.594 ± 0.300	1.816 ± 0.337	0.527 ± 0.177	4.564 ± 0.018	0.735 ± 0.014
Average	-0.890 ∓ 0.142	0.998 ± 0.027	2.719 ± 0.137	0.400 ± 0.036	4.579 ± 0.007	0.934 ± 0.016

[a] Excluding Sk $-69^\circ 256$.

curve is given in Figures 2–4. The effects of the uncertainty in R_V on the CCM relationship are shown in these plots by using dashed curves.

2.6. H I *Columns*

We determined the H I column for each extinction curve by using a variant of the method outlined by Bohlin (1975). This method relies on fitting the wings of the Lyα absorption profile. As we are interested only in a measurement of the difference in the H I column between the reddened and comparison stars, we made this measurement in the ratio spectrum for each reddened and comparison star pair. The uncertainty in this measurement was estimated by eye, varying the H I value until it was noticeably incorrect. Two examples of this are shown in Figure 5. Basically, the strength of a model Lyα profile is adjusted until the division of the ratio spectrum by the model spectrum yields a straight line. The central wavelength of the Lyα line for the LMC and SMC is corrected for the heliocentric velocity of the LMC and SMC (280 and 130 km s^{-1}, respectively). The central region of the Lyα line is ignored as it is contaminated by geocoronal emission. This measurement is straightforward for the STIS data. For *IUE* data, this measurement is much more uncertain as the contamination by geocoronal emission is much larger and the spectra blueward of Lyα are very noisy. The red wing of Lyα was mainly used in the measurement of H I columns for the *IUE* data. The measured H I values and uncertainties are tabulated in Table 2.

3. DISCUSSION

3.1. *Comparison of Magellanic Cloud and Milky Way Extinction Curves*

Now that we have produced full ultraviolet to near-infrared extinction curves [in units of $A(\lambda)/A(V)$] for all the known Magellanic Cloud reddened/comparison star pairs, we can quantitatively compare them with Milky Way extinction curves. The R_V-dependent CCM relationship and the CCM sample extinction curves provides a nice compact form for representing the properties of Milky Way dust found in the local interstellar medium. Thus, we can compare Milky Way and Magellanic Clouds dust by seeing whether the CCM relationship is applicable to any of the individual extinction curves or describes aspects of the sample behavior of these curves.

To test whether the CCM relationship accurately describes any of the individual extinction curves, we

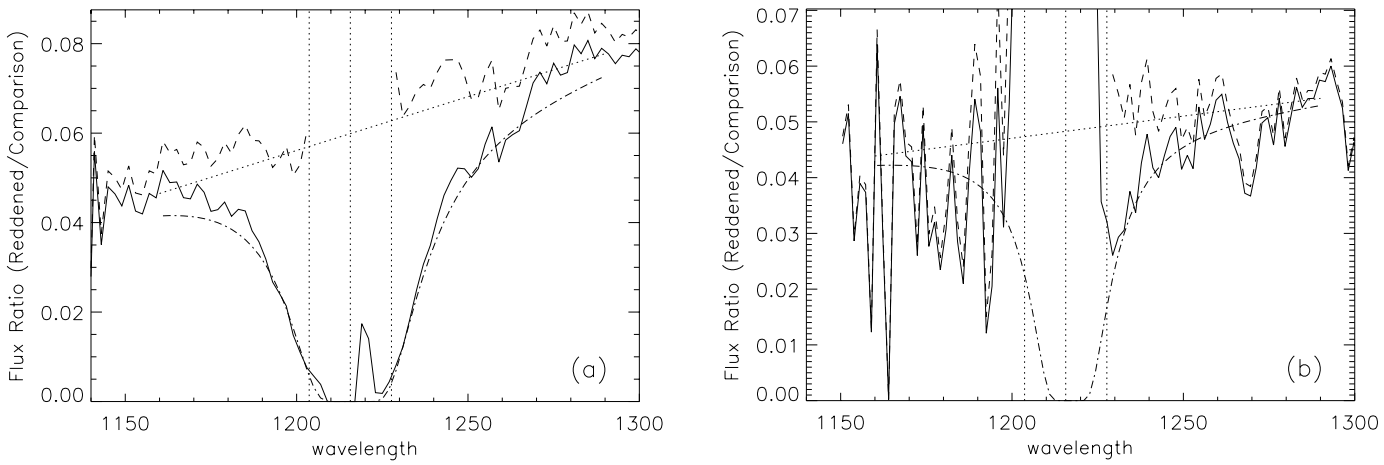

FIG. 5.—Ratio spectra (*solid line*) for (*a*) the AzV 23/404 pair and (*b*) the Sk −69°108/Sk −67°78 pair, shown with the best-fit H I profile (*dot-dashed line*) and the ratio spectrum divided by the best-fit model Lyα profile (*dashed line*). The vertical dotted lines give the center of the Lyα line for the (*a*) SMC and (*b*) LMC velocities and ±12 Å region, which is excluded from the fit. The dotted line gives a nominal continuum.

compare the full measured UV with near-infrared extinction curves with the appropriate CCM curve for the measured R_V. This is done in Figures 2–4 and includes curves showing the uncertainty in the measured curve, as well as the uncertainty in the CCM curve due to uncertainty in the measured R_V value. It should be remembered that the CCM relationship gives the average behavior at a particular R_V and that individual curves can have small deviations from this average behavior and still follow the CCM relationship.

It is clear from Figure 2 that the four curves located in the star-forming bar of the SMC (AzV 18, 23, 214, and 398) do not follow the CCM relationship. For the one curve located outside the SMC bar (AzV 456), the CCM curve does a better job following the measured curve, but there still are significant deviations at the 2175 Å bump and in the far-UV (>7 μm^{-1}). Thus, there are no measured extinction curves in the SMC that follow the CCM relationship.

In the LMC, there are one curve in the LMC2 sample (Sk −69°280) and three curves in the LMC average sample (Sk −66°19, Sk −68°23, and Sk −69°108) that follow the CCM relationship within their uncertainties (Figs. 3–4). Thus, there is evidence that the CCM relationship is at work in the LMC, but only in a limited sense as it describes only four of the 19 measured extinction curves.

The most direct way to quantify how applicable the CCM relationship is in the Magellanic Clouds is to plot R_V^{-1} versus A_λ/A_V. This was how the CCM relationship was originally presented by Cardelli et al. (1989). Figure 6 shows such plots for $\lambda = 1200$, 1500, 2200, and 2800 Å and U and J bands. Since the CCM relationship represents the average extinction behavior as a function of R_V, saying extinction measurements do not follow CCM is to say that they are beyond the scatter of the extinction curves that were used to derive the CCM relationship. In Figure 6, the open circles without error bars give data for the extinction curves used to derive CCM and can be used to determine the scatter that is consistent with the CCM relationship. These plots show that at far-UV wavelengths ($\lambda = 1200$ and 1500 Å) the CCM relationship forms a lower bound to the values of $A(\lambda)/A(V)$ at a particular value of R_V. At longer wavelengths ($\lambda \geq 2200$ Å), the Magellanic Clouds measurements are indistinguishable from the CCM relationship within their uncertainties.

A final way to probe how well the CCM relationship works in the Magellanic Clouds is to examine the behavior of the FM parameters as a function of R_V. The FM parameters describe the UV extinction curve with only six parameters, allowing for more sensitive tests to be performed. The FM parameters C_1, C_2, C_3, and C_4 have a factor of R_V embedded in them. We have plotted the equivalent R_V-independent coefficients versus R_V^{-1} in Figure 7. These R_V-independent coefficients can be derived by examining equation (1) converted from $E(x-V)/E(B-V)$ to $A(x)/A(V)$ units. The equation expressed this way is

$$A(x)/A(V) = \frac{E(x-V)}{E(B-V)}\frac{1}{R_V} + 1 \quad (4)$$

$$= (C_1/R_V + 1) + (C_2/R_V)x + (C_3/R_V)D(x, \gamma, x_0) + (C_4/R_V)F(x)\ . \quad (5)$$

The behavior of the $(C_1/R_V + 1)$, C_2/R_V, C_3/R_V, and C_4/R_V coefficients do not follow the CCM relationship directly, but the CCM relationship does form a bound on the values of these coefficients as a function of R_V. For example, all the values of C_2/R_V lie on or above the line defining the CCM relationship. In the plots of the other three coefficients, the CCM relationship forms an upper bound on their behaviors. In the case of x_0 and γ, CCM does not predict much of a dependence on R_V, and we do not see one for the Magellanic Clouds either. The values of x_0 and γ for the Magellanic Clouds have a much larger scatter than seen in the extinction curves defining CCM. For x_0 this scatter is consistent with the uncertainties in x_0. For γ, the scatter is larger than can be accounted for by measurement uncertainties. Thus, it is either real or the result of measurement uncertainties we have not accounted for in our error analysis.

By examining the behavior of the Magellanic Cloud extinction curves with R_V in three different ways and comparing that behavior with that predicted by the R_V-dependent CCM relationship, we find evidence that the general behavior of Milky Way extinction curves is seen in the Magellanic Clouds. Not only are four LMC extinction curves indistinguishable from Milky Way extinction curves, but the general behavior of Milky Way extinction curves

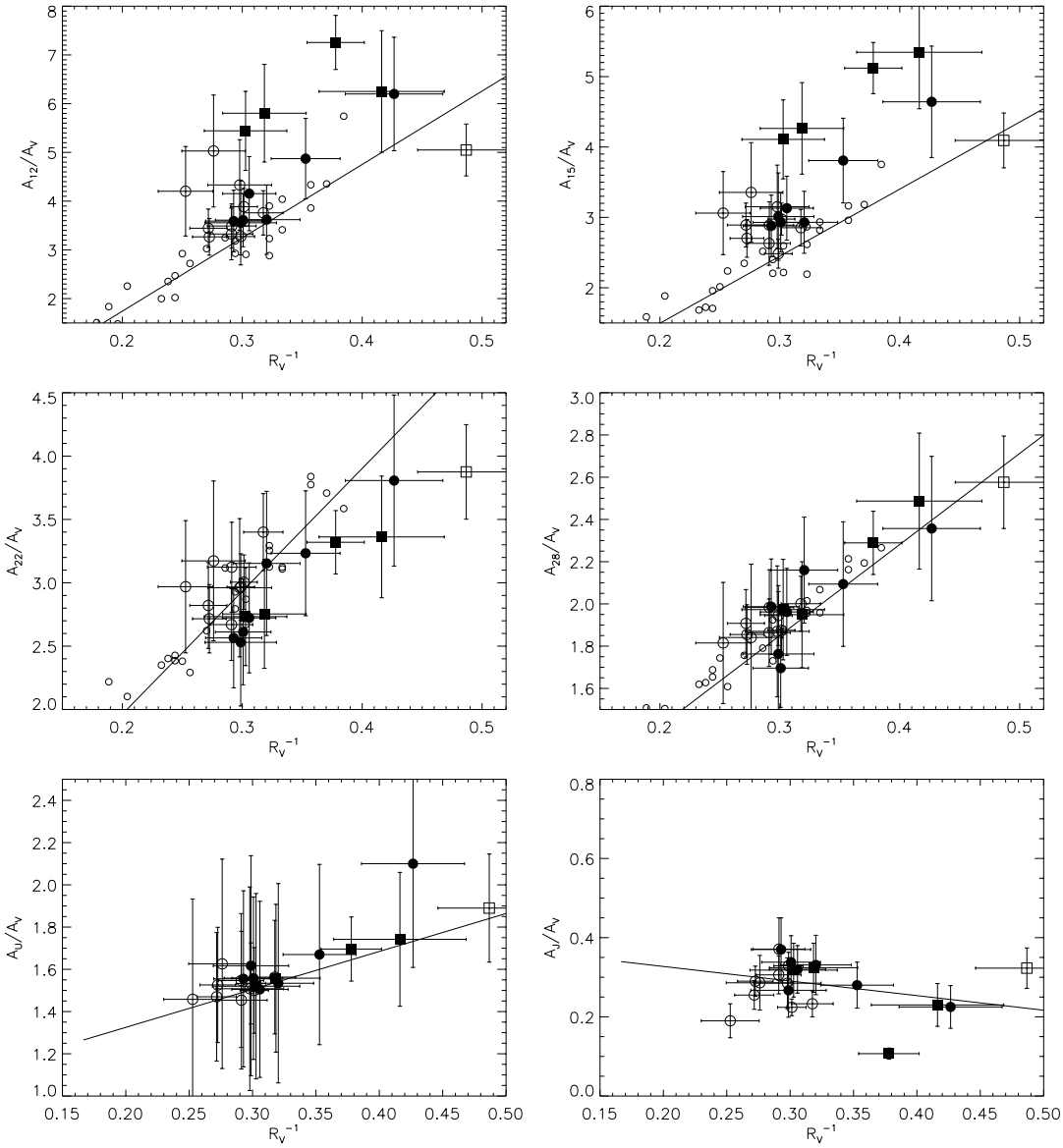

FIG. 6.—Plots of A_λ/A_V vs. R_V^{-1} for $A_{12} = A$ (1200 Å), $A_{15} = A$ (1500 Å), $A_{22} = A$ (2200 Å), $A_{28} = A$ (2800 Å), $A_U = A$ (3500 Å, U band), and $A_J = A$ (1.25 μm, J band). The LMC and SMC measurements are given by filled circles for the average, open circles for LMC2, filled squares for the bar, and open squares for the wing, with error bars, respectively. The line gives the CCM relationship, and the open circles without error bars the original Fitzpatrick & Massa (1990) data used by CCM ($\lambda < 3000$ Å plots only).

forms a bound on the general behavior of Magellanic Cloud extinction curves.

3.2. *Super-CCM Relationship?*

While a small number of Magellanic Cloud extinction curves do seem to be well described by the CCM relationship, the majority do not. Yet there is strong evidence that the CCM relationship serves as a bound on the behavior of all the Magellanic Cloud extinction curves. This fact raises the question: Is there some more general relationship dependent on R_V and at least one other parameter that describes the average behavior of the Milky Way and Magellanic Cloud extinction curves?

An indication that such a relationship might exist was presented by Clayton et al. (2000) for low-density sight lines in the Milky Way that display some of the same deviations from CCM seen in the Magellanic Clouds. They found that the strength of the 2175 Å bump ($\pi C_3/2\gamma$) and the steepness of the ultraviolet extinction (C_2) were anticorrelated along the low-density sight lines, as well as for the average curves in the Magellanic Clouds (Gordon & Clayton 1998; Misselt et al. 1999). We present a similar plot in Figure 8 for the Magellanic Cloud extinction curves with the equivalent R_V-independent measures of the 2175 Å bump strength and ultraviolet extinction steepness. This plot gives evidence for an anticorrelation between the strength of the 2175 Å bump and the steepness of the ultraviolet extinction.

One possible second parameter could be the measured gas-to-dust ratio [$N(\mathrm{H\ I})/A(V)$]. To test this we have plotted in Figure 9 the gas-to-dust ratios versus the 2175 Å bump strength and ultraviolet steepness values for the Magellanic Cloud extinction curves. The scatter in these two plots is quite large as are the uncertainties on the individual points.

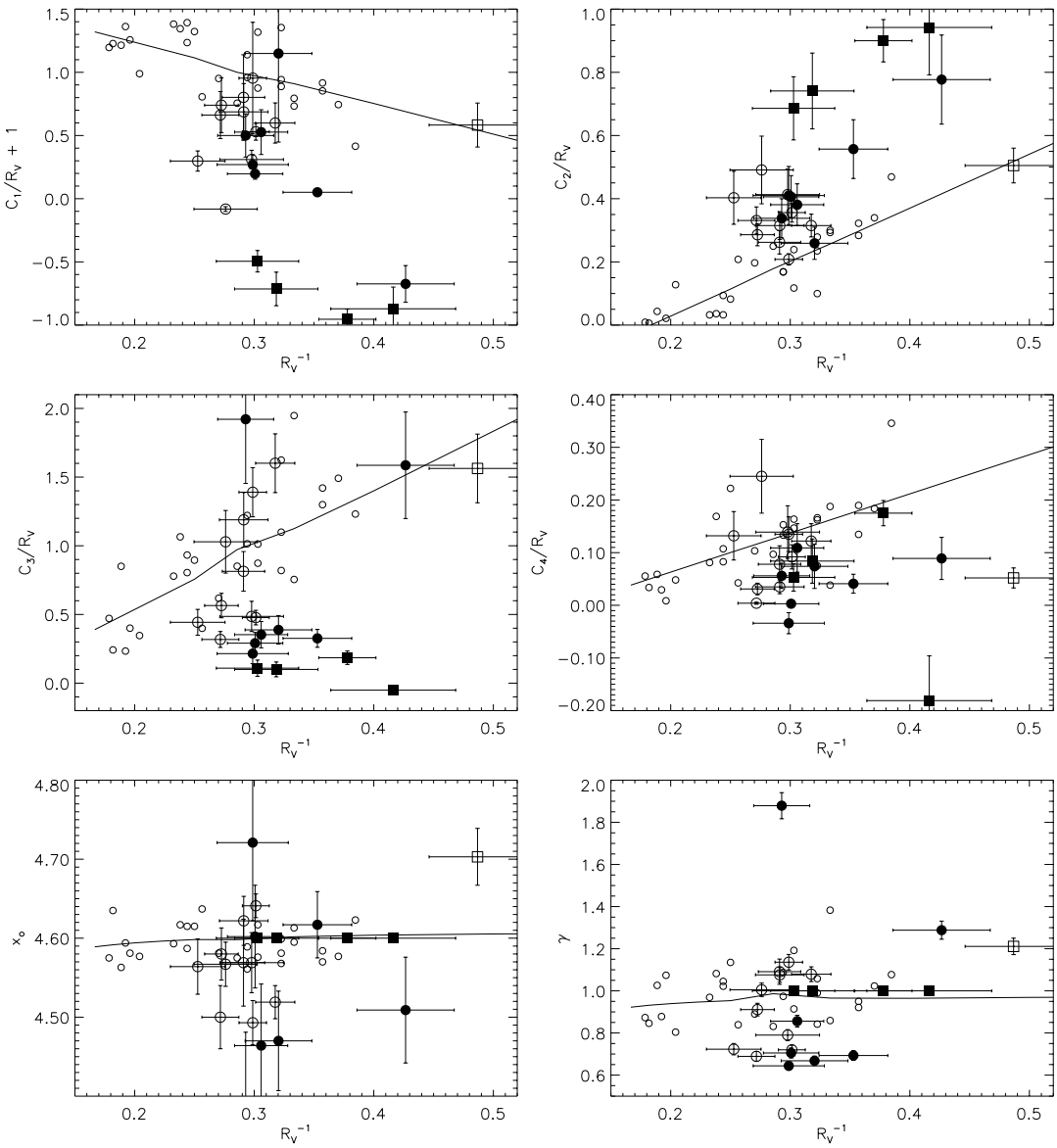

FIG. 7.—FM fit parameters plotted vs. R_V^{-1}, The LMC and SMC measurements are given by filled circles for the average, open circles for LMC2, filled squares for the bar, and open squares for the wing, with error bars, respectively. The line gives the CCM relationship and the open circles without error bars the original Fitzpatrick & Massa (1990) data used by CCM.

There might be real correlations in both plots, but higher quality data are needed. There would be reason to expect a correlation between the gas-to-dust ratio and the behavior of extinction curves. The gas-to-dust ratio is known to correlate with metallicity on a galaxy-wide basis (Issa, MacLaren, & Wolfendale 1990). On a local scale, it could be a measure of the formation and destruction history of dust grains. For example, the dust self-shielding will decrease with increasing gas-to-dust ratio, making it easier for dust grains to be destroyed by the ambient radiation field. If the dust grains responsible for the 2175 Å bump are easier to destroy than those responsible for the underlying ultraviolet extinction, a behavior like that seen in Figure 9 would be expected.

3.3. *SMC Bar Extinction Curves and the* 2175 Å *Bump*

The extremely weak or absent 2175 Å bump in the four SMC bar extinction curves makes these curves unique. In all other measured extinction curves, the 2175 Å bump is quite prominent. The obvious question is whether the weak 2175 Å bump in the SMC bar is due to Milky Way contamination or is intrinsic to the SMC. While only one of the four curves has a bump that is detected at greater than 3 σ, the other three are all 2 σ detections. The construction of the curves by using SMC comparison stars should remove all the Milky Way foreground, but small differences between the reddened and comparison stars foreground could result in a weak 2175 Å bump. A foreground contamination such as this would result in a positive bump as often as a negative bump. Interestingly, one of the four SMC bump curves (AzV 214) has a 2 σ detection of a negative bump and a negative far-UV curvature (C_4). The foreground contamination [in percent of total $E(B-V)$ with 1 σ uncertainties] needed to produce spurious bump detections at the observed levels would have to be 25% ± 14%, 39% ± 10%, 10% ± 5%, and 23% ± 13% for AzV 18, 23, 214, and 398, respectively.

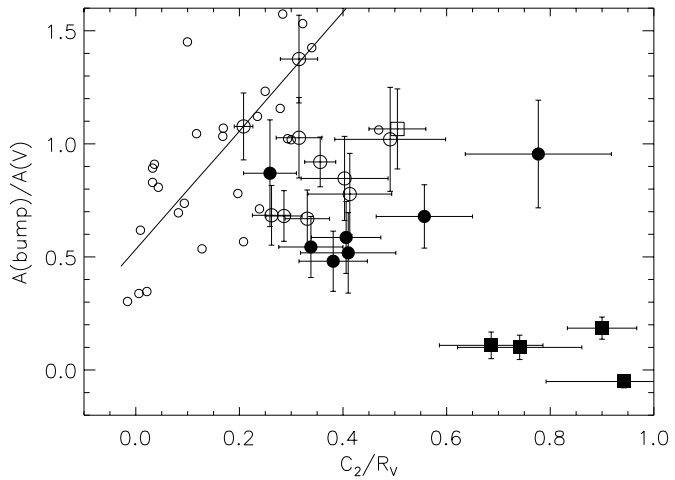

FIG. 8.—Strength of the 2175 Å bump [$A(\mathrm{bump})/A(V) = C_3/\gamma^2 R_V$] vs. the steepness of the ultraviolet extinction (C_2/R_V). The LMC and SMC measurements are given by filled circles for the average, open circles for LMC2, filled squares for the bar, and open squares for the wing, with error bars, respectively. The line gives the CCM relationship, and the open circles without error bars the original Fitzpatrick & Massa (1990) data used by CCM.

These foreground contaminations are not unlikely given the low $E(B-V)$ values for these sight lines, especially given the large uncertainties. While it is difficult to definitively decide, the current evidence suggests that the carriers of the 2175 Å bump could be completely absent from the dust in the SMC bar sight lines.

3.4. *Sample Average Curves*

Since the Magellanic Cloud extinction curves display significantly different shapes than that seen in the Milky Way, average extinction curves of the LMC average, LMC2 supershell, and SMC bar samples are of interest. These average curves capture the large-scale variations in dust properties at higher signal-to-noise ratio than the individual curves.

While past work has produced such average curves (Gordon & Clayton 1998; Misselt et al. 1999), we can create more accurate average curves as the result of our determinations of R_V values. We have averaged the individual curves in each sample in $A(\lambda)/A(V)$ units instead of $E(\lambda-V)/E(B-V)$ units as was done in previous work. $E(\lambda-V)/E(B-V)$ units are a relative measure of dust properties whereas $A(\lambda)/A(V)$ units are an absolute measure of the dust properties and, as a result, more accurately represent the effects of dust. For the LMC2 supershell sample, we have not used the results for Sk $-69°256$ in producing the LMC2 supershell average. Its extremely low R_V value of 0.64 is likely the result of poor *JHK* photometry, contamination by nearby hot dust, or contamination by a red companion.

The sample average curves are given in Figure 10 and tabulated in Table 4. The averages were calculated by weighting by the uncertainties at each wavelength for each individual curve and in 0.25 $\mu\mathrm{m}^{-1}$ wide bins. The average values of R_V and $N(\mathrm{H\ I})/A(V)$ were also calculated by weighting by the individual uncertainties and are tabulated in Table 2. The average curves were fitted with the FM parameterization and the best-fit six FM parameters are given in Table 3. The FM fits were done for wavelengths less than 8.4 $\mu\mathrm{m}^{-1}$ as this is the bluest wavelength common to the *IUE* and STIS data. This fitting limit affected only the SMC bar average.

For the SMC bar, we find that $R_V = 2.74 \pm 0.13$ and $N(\mathrm{H\ I})/A(V) = 13.18 \pm 1.02$, which is consistent with the results of Bouchet et al. (1985) and Gordon & Clayton (1998). However, we do not find that the gas-to-dust ratio for AzV 456 (Sk 143) is similar to that of the Milky Way. For the Milky Way, $N(\mathrm{H\ I})/A(V) \sim 1.55$ (Bohlin, Savage, & Drake 1978; Diplas & Savage 1994), and we find $N(\mathrm{H\ I})/A(V) = 7.40 \pm 1.20$ for AzV 456 whereas Bouchet et al. (1985) found $N(\mathrm{H\ I})/A(V) \sim 2.6$ by assuming $R_V = 2.72$ (the average R_V for the entire SMC). The differences between our measurement and Bouchet et al. (1985) can be traced to our lower $E(B-V)$ and a lower R_V value. These differences illustrate the difficulties of measuring such quantities for low-reddening sight lines.

For the LMC2 supershell sample, we find that $R_V = 2.76 \pm 0.09$ and $N(\mathrm{H\ I})/A(V) = 6.97 \pm 0.67$. Our gas-to-dust ratio is roughly consistent with results of

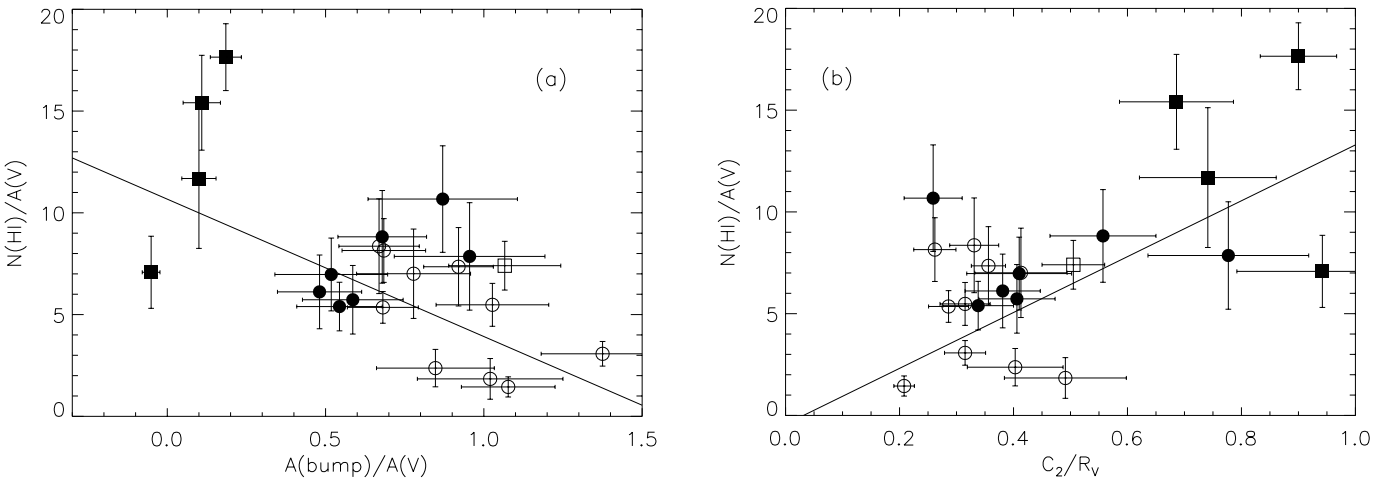

FIG. 9.—Behavior of the gas-to-dust ratios [$N(\mathrm{H\ I})/\mathrm{A(V)}$] vs. (*a*) the 2175 Å bump strength [$A(\mathrm{bump})/A(V)$] and (*b*) the ultraviolet steepness (C_2/R_V). The LMC and SMC measurements are given by filled circles for the average, open circles for LMC2, filled squares for the bar, and open squares for the wing, with error bars, respectively. The line gives a simple linear fit to the data.

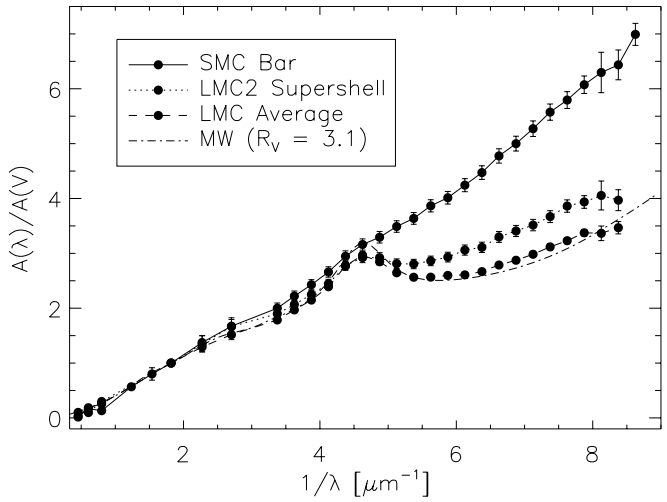

FIG. 10.—Sample average extinction curves plotted along with the "average" Milky Way curve (CCM with $R_V = 3.1$).

Koornneef (1982) and Fitzpatrick (1985), who found $N(\mathrm{H\ I})/A(V) \sim 6.3$ and 8.7, respectively. Our value of R_V is lower than that of Clayton & Martin (1985), who found $R_V \sim 3.5$ but consistent with Misselt et al. (1999). For the LMC average sample, we find that $R_V = 3.41 \pm 0.06$ and $N(\mathrm{H\ I})/A(V) = 3.25 \pm 0.28$. These values are significantly different from those for the LMC2 supershell sample. The different gas-to-dust ratios are in conflict with the conclusions of Fitzpatrick (1986), who state that there are no gas-to-dust measurable differences between the non–30 Dor and 30 Dor samples. However, examination of their Figure 6 shows that the non–30 Dor points fall consistently below the 30 Dor gas-to-dust ratio, implying that we are not in conflict with earlier work. The lower gas-to-dust ratio is especially interesting as it supports a systematic trend of more extreme extinction curves (smaller 2175 Å bump and steeper far-UV rise) with rising gas-to-dust ratio (see § 3.2).

4. CONCLUSIONS

We have presented a quantitative exhaustive comparison of all the known Magellanic Cloud extinction curves with a representative sample of Milky Way extinction curves. Like previous studies (Nandy & Morgan 1978; Lequeux et al. 1982; Prèvot et al. 1984; Clayton & Martin 1985; Fitzpatrick 1986; Gordon & Clayton 1998; Misselt et al. 1999), we find that both the LMC and SMC have examples of extinction curves qualitatively similar to those found in the Milky Way. Unlike previous studies, we are able to take this comparison one step further and make quantitative comparisons as we determined R_V values for all Magellanic Cloud extinction curves. This allows the comparison of Magellanic Cloud and Milky Way extinction curves to be done using measurements based on absolute dust properties

TABLE 4
SAMPLE AVERAGE CURVES

λ (μm)	x (μm^{-1})	$A(\lambda)/A(V)$		
		SMC Bar	LMC2 Supershell	LMC Average
2.198	0.455	0.016 ± 0.003	0.101 ± 0.003	0.030 ± 0.003
1.650	0.606	0.169 ± 0.020	0.097 ± 0.020	0.186 ± 0.020
1.250	0.800	0.131 ± 0.013	0.299 ± 0.013	0.257 ± 0.013
0.810	1.235	0.567 ± 0.048	...	...
0.650	1.538	0.801 ± 0.113	...	...
0.550	1.818	1.000 ± 0.046	1.000 ± 0.048	1.000 ± 0.048
0.440	2.273	1.374 ± 0.127	1.349 ± 0.113	1.293 ± 0.113
0.370	2.703	1.672 ± 0.123	1.665 ± 0.046	1.518 ± 0.046
0.296	3.375	2.000 ± 0.095	1.899 ± 0.127	1.786 ± 0.127
0.276	3.625	2.220 ± 0.093	2.067 ± 0.123	1.969 ± 0.123
0.258	3.875	2.428 ± 0.093	2.249 ± 0.095	2.149 ± 0.095
0.242	4.125	2.661 ± 0.095	2.447 ± 0.093	2.391 ± 0.093
0.229	4.375	2.947 ± 0.099	2.777 ± 0.093	2.771 ± 0.093
0.216	4.625	3.161 ± 0.102	2.922 ± 0.095	2.967 ± 0.095
0.205	4.875	3.293 ± 0.104	2.921 ± 0.099	2.846 ± 0.099
0.195	5.125	3.489 ± 0.105	2.812 ± 0.102	2.646 ± 0.102
0.186	5.375	3.637 ± 0.107	2.805 ± 0.104	2.565 ± 0.104
0.178	5.625	3.866 ± 0.112	2.863 ± 0.105	2.566 ± 0.105
0.170	5.875	4.013 ± 0.115	2.932 ± 0.107	2.598 ± 0.107
0.163	6.125	4.243 ± 0.119	3.060 ± 0.112	2.607 ± 0.112
0.157	6.375	4.472 ± 0.124	3.110 ± 0.115	2.668 ± 0.115
0.151	6.625	4.776 ± 0.131	3.299 ± 0.119	2.787 ± 0.119
0.145	6.875	5.000 ± 0.135	3.408 ± 0.124	2.874 ± 0.124
0.140	7.125	5.272 ± 0.142	3.515 ± 0.131	2.983 ± 0.131
0.136	7.375	5.575 ± 0.148	3.670 ± 0.135	3.118 ± 0.135
0.131	7.625	5.795 ± 0.153	3.862 ± 0.142	3.231 ± 0.142
0.127	7.875	6.074 ± 0.160	3.937 ± 0.148	3.374 ± 0.148
0.123	8.125	6.297 ± 0.368	4.055 ± 0.153	3.366 ± 0.153
0.119	8.375	6.436 ± 0.271	3.969 ± 0.160	3.467 ± 0.160
0.116	8.625	6.992 ± 0.201	...	...

$[A(\lambda)/A(V)]$ instead of relative dust properties $[E(\lambda - V)/E(B - V)]$. The importance of this difference is well illustrated by the work of Cardelli et al. (1989) in which the comparison of Milky Way curves in $A(\lambda)/A(V)$ units allowed for the derivation of the R_V-dependent CCM relationship. We conclude that four extinction curves in the LMC are *indistinguishable* from Milky Way extinction curves and Milky Way extinction curves form a bound on the behavior of Magellanic Cloud extinction curves.

The majority of the Magellanic Cloud extinction curves are significantly different from Milky Way extinction curves, and this is likely a result of Magellanic Cloud extinction curves probing quite different environments than the CCM sample of Milky Way extinction curves. The CCM sample is based on fairly quiescent sight lines, and most of our extinction curve measurements in the Magellanic Clouds are biased toward quite active regions as they are based on OB supergiants. The systematic behavior of the curves studied in this paper hint at the existence of a multiparameter relationship [possibly dependent on R_V and $N(\mathrm{H\ I})/A(V)$] describing both quiescent (CCM-like) and active extinction curves.

The different biases between the majority of the measured Milky Way and Magellanic Cloud extinction curves point to a weakness in our understanding of dust properties. The Magellanic Cloud extinction curves are biased toward active star-forming regions (OB supergiant sight lines) and low dust columns. The Milky Way sight lines are less biased toward active star-forming regions as they are mainly measured along sight lines toward OB main-sequence stars. They are limited in their variety of dust properties probed as the measurements are generally limited to our local region of the Milky Way. Evidence that the type of dust seen in the Magellanic Clouds does exist in the Milky Way is seen along Milky Way low-density sight lines (Clayton et al. 2000). Higher dust column sight lines and sight lines toward main-sequence stars need to be measured in the Magellanic Clouds to allow us to truly explore the possible range of dust properties.

The results of this work and those of Clayton et al. (2000) imply that the common usage of discussing Milky Way, LMC, and SMC dust as separate is inaccurate. In reality, a continuum of dust properties exists between that seen in the quiescent and active regions (e.g., see Fig. 8). The usual average curves can then be arranged into a rough version of this sequence, and it would be Milky Way (CCM), LMC average, SMC wing (AzV 456), LMC2 supershell, and SMC bar. Ordering all the individual known extinction curves would produce an even greater mixing of Milky Way, LMC, and SMC curves. This work describes a qualitative view of the continuum of dust extinction curves. Quantifying the variation between quiescent and active region extinction curves would give valuable clues to the identities of dust grain properties.

Support for proposal 8198 was provided by NASA through a grant from the Space Telescope Science Institute, which is operated by the Association of Universities for Research in Astronomy, Inc., under NASA contract NAS 5-26555. We thank the referee for comments that motivated us to improve the presentation of this paper. This work was partially supported through JPL contract 960785. A. U. L. acknowledges support from NSF grant AST 00-97895. This publication makes use of data products from the Two Micron All-Sky Survey, which is a joint project of the University of Massachusetts and the Infrared Processing and Analysis Center, California Institute of Technology, funded by the National Aeronautics and Space Administration and the National Science Foundation. This research made use of the SIMBAD database and VizieR catalog access tool, CDS, Strasbourg, France.

APPENDIX

R_V VALUE AND UNCERTAINTY EQUATIONS

The derivation of the equations to determine value of R_V and its uncertainty are given in this appendix. To the knowledge of the authors, these equations have not appeared in the literature before and are included in this paper as they may be of use to others. The equations below are equivalent to determining R_V from individual colors and averaging the results weighted by the appropriate uncertainties.

The equation giving the χ^2 between the measured extinction curve and the Rieke & Lebofsky (1985) curve is

$$\chi^2 = \sum_i \left[\frac{y(\lambda_i) - y(R_V, \lambda_i)}{\sigma(\lambda_i)} \right]^2 , \tag{A1}$$

where

$$y(\lambda_i) = E(\lambda_i - V)/E(B - V) , \tag{A2}$$

$$\sigma(\lambda_i) = \sigma E(\lambda_i - V)/E(B - V) , \tag{A3}$$

$$y(R_V, \lambda_i) = [A(\lambda_i)/A(V) - 1]R_V , \tag{A4}$$

and $A(\lambda_i)/A(V)$ is given in Table 3 of Rieke & Lebofsky (1985). Differentiating χ^2 with respect to R_V and setting the result to zero gives

$$R_V = \frac{\sum_i [A(\lambda_i)/A(V) - 1]}{\sum_i \left[y(\lambda_i)/\sigma(\lambda_i)^2 \right]} . \tag{A5}$$

Using equation (6.19) of Bevington & Robinson (1992) gives the uncertainty in R_V as

$$\sigma(R_V)^2 = \frac{\sum_i [A(\lambda_i)/A(V) - 1]}{\sum_i \left\{ [A(\lambda_i)/A(V) - 1]^2 / \sigma(\lambda_i)^2 \right\}} \ . \tag{A6}$$

REFERENCES

Aiello, S., Barsella, B., Chlewicki, G., Greenberg, J. M., Patriarchi, P., & Perinotto, M. 1988, A&AS, 73, 195
Bevington, P. R., & Robinson, D. K. 1992, Data Reduction and Error Analysis for the Physical Sciences (New York: McGraw-Hill)
Bohlin, R. 1975, ApJ, 200, 402
Bohlin, R. C., Savage, B. D., & Drake, J. F. 1978, ApJ, 224, 132
Bouchet, P., Lequeux, J., Maurice, E., Prevot, L., & Prevot-Burnichon, M. L. 1985, A&A, 149, 330
Cardelli, J. A., Clayton, G. C., & Mathis, J. S. 1989, ApJ, 345, 245
Cioni, M.-R., et al. 2000, A&AS, 144, 235
Clayton, G. C., Gordon, K. D., & Wolff, M. J. 2000, ApJS, 129, 147
Clayton, G. C., & Martin, P. G. 1985, ApJ, 288, 558
Cutri, R. M., et al. 2000, Explanatory Supplement to the 2MASS Second Incremental Data Release (Pasadena: IPAC)
Diplas, A., & Savage, B. D. 1994, ApJ, 427, 274
Epchtein, N., et al. 1999, A&A, 349, 236
Fitzpatrick, E. L. 1985, ApJ, 299, 219
———. 1986, AJ, 92, 1068
Fitzpatrick, E. L., & Massa, D. 1988, ApJ, 328, 734
Fitzpatrick, E. L., & Massa, D. 1990, ApJS, 72, 163
Gordon, K. D., & Clayton, G. C. 1998, ApJ, 500, 816
Issa, M. R., MacLaren, I., & Wolfendale, A. W. 1990, A&A, 236, 237
Koornneef, J. 1982, A&A, 107, 247
Landolt, A. U. 1992, AJ, 104, 340
Lequeux, J., Maurice, E., Prévot-Burnichon, M.-L., Prévot, L., & Rocca-Volmerange, B. 1982, A&A, 113, L15
Martin, P. G., & Whittet, D. C. B. 1990, ApJ, 357, 113
Massa, D., & Fitzpatrick, E. L. 2000, ApJS, 126, 517
Mathis, J. S., & Cardelli, J. A. 1992, ApJ, 398, 610
Misselt, K. A., Clayton, G. C., & Gordon, K. D. 1999, ApJ, 515, 128
Morgan, D. H., & Nandy, K. 1982, MNRAS, 199, 979
Nandy, K., & Morgan, D. H. 1978, Nature, 276, 478
Prèvot, M. L., Lequeux, J., Maurice, E., Prèvot, L., & Rocca-Volmerange, B. 1984, A&A, 132, 389
Rieke, G. H., & Lebofsky, M. J. 1985, ApJ, 288, 618
Skrutskie, M. F., et al. 1997, in The Impact of Large Scale Near-IR Sky Surveys (Dordrecht: Kluwer), 25
Witt, A. N., Bohlin, R. C., & Stecher, T. P. 1984, ApJ, 279, 698